ChemComm

COMMUNICATION

View Article Online
View Journal | View Issue

Cite this: *Chem. Commun.*, 2015, 51, 9659

Received 18th March 2015,
Accepted 11th May 2015

DOI: 10.1039/c5cc02282g

www.rsc.org/chemcomm

Chemical decoration of $CH_3NH_3PbI_3$ perovskites with graphene oxides for photodetector applications†

Minhong He,‡ Yani Chen,‡ Hui Liu, Jialin Wang, Xiaosheng Fang and Ziqi Liang*

A facile *in situ* solution method was developed for chemical decoration of $CH_3NH_3PbI_3$ perovskites with reduced graphene oxides (rGOs) to significantly improve the photodetector performance. Such $CH_3NH_3PbI_3$/rGO molecular hybrids show a 6 times higher ON/OFF ratio and notably faster response speed than neat $CH_3NH_3PbI_3$.

Organolead halide perovskites ($CH_3NH_3PbX_3$, X = halogen I, Br, Cl) have very recently drawn intensive research interest due to their fascinating features such as large light absorption coefficients, a broad absorption range, high carrier mobility, customizable optical properties and superior solution processability.[1–7]

Nowadays, many newly developed high-performance optical devices such as solar cells and photodetectors are based on perovskite thin films.[8–15] These thin films can be prepared through one-step precursor solution deposition,[1] two-step sequential deposition,[16] dual-source vapor deposition[17] and vapor assisted solution processes.[18] The resulting devices are usually in a bilayer heterojunction architecture other than a bulk heterojunction (BHJ) structure where rich interfaces are created for efficient charge separation and transport. However, such BHJ structure is extremely difficult to construct due to miscibility issues. One alternatively effective approach to such BHJ construction is to generate the free-standing perovskite based p–n molecular junctions.

Herein, we report a simple and versatile solution method toward chemical decoration of $CH_3NH_3PbI_3$ perovskites to obtain such free-standing perovskite based molecular hybrids. Solution-processable reduced graphene oxide (rGO) has been widely used for optoelectronic devices because of its large specific surface area and high charge mobility.[19–21] As a proof-of-concept, we constructed a $CH_3NH_3PbI_3$/rGO hybrid based photodetector, which exhibited the ON/OFF ratio 6 times higher than that based on neat $CH_3NH_3PbI_3$. Moreover, the hybrid photodetector displayed notably faster response speed of both the rise and decay time than the neat one. Importantly, this work offers a controllable and facile strategy for design and *in situ* synthesis of perovskite based nanocomposites.

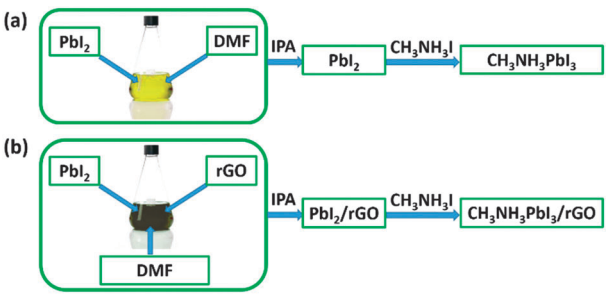

Fig. 1 Schematic illustration of (a) synthesis of $CH_3NH_3PbI_3$ and (b) *in situ* synthesis of $CH_3NH_3PbI_3$/rGO hybrids.

Synthetic routes towards free-standing $CH_3NH_3PbI_3$ and $CH_3NH_3PbI_3$/rGO hybrids are schematically depicted in Fig. 1. The experimental details are described in the ESI.† As shown in Fig. 1a, $CH_3NH_3PbI_3$ was prepared by the following steps. PbI_2 was first fully dissolved in DMF, followed by dropwise addition of isopropanol (IPA), which is anti-solvent of PbI_2, yielding a suspension. A stoichiometric excess of CH_3NH_3I was then added into the PbI_2 suspension and stirred under ambient conditions. The colour of the suspension transformed gradually from yellow to black, indicating the formation of $CH_3NH_3PbI_3$. Fig. 1b shows the steps of *in situ* synthesis of $CH_3NH_3PbI_3$/rGO hybrids. The rGO was synthesized according to our recent procedures.[22] PbI_2 and rGO were mixed in a DMF solution, to which IPA was dropwise added as anti-solvent to yield the suspension of rGO/PbI_2 hybrids. The rGO/PbI_2 was then redispersed in IPA, followed by addition of excessive CH_3NH_3I under stirring at room temperature. The suspension then turned from yellow to black, implying the successful *in situ* transformation from PbI_2/rGO to $CH_3NH_3PbI_3$/rGO. Finally, the $CH_3NH_3PbI_3$/rGO hybrid solids were collected by precipitation in hexane and washing with IPA, followed by centrifugation. It is estimated that about 0.3 wt% rGO is in the final $CH_3NH_3PbI_3$/rGO products. Note that we have also successfully applied this

Department of Materials Science, Fudan University, Shanghai 200433, China. E-mail: zqliang@fudan.edu.cn

† Electronic supplementary information (ESI) available: Experimental section and Fig. S1 and S2. See DOI: 10.1039/c5cc02282g

‡ These authors contributed equally to this work.

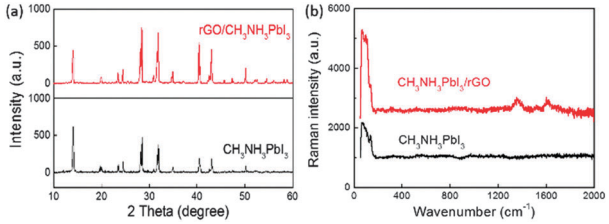

Fig. 2 (a) XRD patterns and (b) Raman spectra of free-standing neat $CH_3NH_3PbI_3$ and $CH_3NH_3PbI_3$/rGO hybrids.

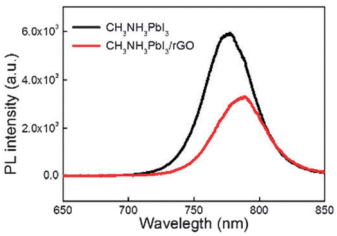

Fig. 4 Comparison of solid-state PL spectra of neat $CH_3NH_3PbI_3$ and $CH_3NH_3PbI_3$/rGO hybrids.

method to the synthesis of other perovskite nanocomposites such as $CH_3NH_3PbI_3$/Ag nanoparticles.

In order to confirm whether chemical decoration of $CH_3NH_3PbI_3$ with rGO is successful, we investigated the crystalline structures by X-ray diffraction (XRD) measurements. As shown in Fig. 2a, $CH_3NH_3PbI_3$/rGO hybrids show strong peaks at 13.95, 14.09, 19.92, 23.46, 24.47, 28.13, 28.44, 30.89, 31.59, 31.85, 40.43 and 43.03 degrees, corresponding to the reflections from (002), (110), (112), (211), (202), (004), (220), (213), (114), (310), (224) and (314) lattice planes of the perovskite structure, respectively.[23] However, no obvious characteristic peaks of rGO are observed due to its small amount in the hybrids. Moreover, the intensities of all the peaks except for 14.09° in $CH_3NH_3PbI_3$/rGO hybrids are much stronger than that of neat $CH_3NH_3PbI_3$, implying the remarkably improved crystallinity with the aid of rGO. Raman spectra of neat $CH_3NH_3PbI_3$ and $CH_3NH_3PbI_3$/rGO hybrids are also shown in Fig. 2b. Apart from typical peaks of $CH_3NH_3PbI_3$,[24] $CH_3NH_3PbI_3$/rGO hybrids present two additional bands at 1353 and 1598 cm^{-1}, corresponding to D and G bands of rGO, respectively,[25] confirming the successful inclusion of rGO in $CH_3NH_3PbI_3$.

Field-effect scanning electron microscopy (FE-SEM) and transmission electron microscopy (TEM) imaging were then carried out to investigate the morphological variations between neat $CH_3NH_3PbI_3$ and $CH_3NH_3PbI_3$/rGO hybrids. As shown in Fig. 3, both $CH_3NH_3PbI_3$ and $CH_3NH_3PbI_3$/rGO exhibit well-defined cuboid shapes. $CH_3NH_3PbI_3$ crystals show an average diameter of ~200 nm (Fig. 3a), while $CH_3NH_3PbI_3$/rGO particles display a larger size of ~1 μm (Fig. 3b). Larger sized perovskite crystals would favour the charge transport in optoelectronic devices.[26] However, the exact mechanism for the increased crystal size remains unclear in our work. It is also evidently shown that $CH_3NH_3PbI_3$ crystals are distributed along the surfaces of rGO flakes, as displayed in Fig. 2b and Fig. S1.† In addition, TEM images (Fig. S2†) further confirm the presence of rGO at the surfaces of $CH_3NH_3PbI_3$ crystals.

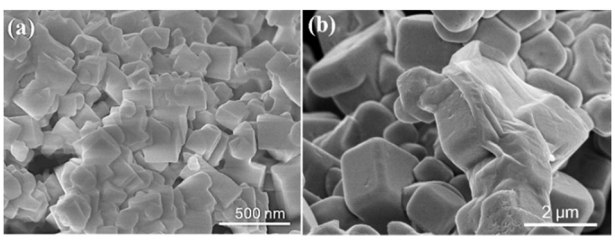

Fig. 3 SEM images of (a) $CH_3NH_3PbI_3$ and (b) $CH_3NH_3PbI_3$/rGO hybrids.

Steady-state photoluminescence (PL) emission spectra were further used to elucidate the role of rGO in $CH_3NH_3PbI_3$/rGO molecular hybrids. Fig. 4 compares the solid-state PL spectra of neat $CH_3NH_3PbI_3$ and $CH_3NH_3PbI_3$/rGO hybrids. The emission peak of $CH_3NH_3PbI_3$/rGO displays a red-shift of 10 nm than that of $CH_3NH_3PbI_3$, indicating the strong interaction between $CH_3NH_3PbI_3$ and rGO. Furthermore, the maximum PL intensity of the hybrids is quenched by 44% compared to that of neat $CH_3NH_3PbI_3$. This dramatic PL quenching is believed to result from efficient charge transfer between the perovskite and graphene.[27–29]

Finally, to demonstrate the effects of efficient charge transfer among $CH_3NH_3PbI_3$/rGO hybrids, photodetectors based on both neat $CH_3NH_3PbI_3$ and hybrids were fabricated. In the literature reports, single-layer $CH_3NH_3PbI_3$ based photodetectors were found to exhibit extremely slow response.[30] On the other hand, it was recently shown that Cu–Ni nanoparticle-decorated rGO hybrid based photodetectors exhibited a quick photoresponse and large photocurrent under white light illumination.[31] This sizable photocurrent generation may be attributed to photothermoelectric and photovoltaic effects *via* the formation of a p–n junction near the metal graphene contacts, thereby enhancing the hot carriers in the system. It is therefore anticipated that by forming p–n molecular junctions, our $CH_3NH_3PbI_3$/rGO hybrids would show impressive photodetector performance.

As shown in Fig. 5a, the photodetectors were prepared by drop-casting of the perovskite suspensions on the Si/SiO_2 substrate, above which the Au/Cr (100/10 nm) electrodes were thermally deposited with a bridging-gap width of ~100 μm and a length of ~120 μm, respectively. Fig. 5b displays the energy level diagram of a $CH_3NH_3PbI_3$/rGO photodetector. On one hand, the $CH_3NH_3PbI_3$/rGO hybrids form p–n molecular junctions with rich interfaces, which lead to efficient charge separation. On the other hand, the insertion of rGO lowers the energy offset between $CH_3NH_3PbI_3$ and Au, which facilitates charge collection. As a result, typical *I–V* curves of $CH_3NH_3PbI_3$ and $CH_3NH_3PbI_3$/rGO photodetectors are shown in Fig. 5c and d, respectively. At a bias of 5 V, the dark currents of $CH_3NH_3PbI_3$ and $CH_3NH_3PbI_3$/rGO (0.3 wt%) photodetectors are very close, that is, 0.19×10^{-9} A and 0.17×10^{-9} A, respectively. However, under light irradiation at 520 nm with an intensity of 3.2 mW cm^{-2}, the $CH_3NH_3PbI_3$/rGO photodetector exhibits a photocurrent of 28.56×10^{-9} A, which is notably larger than that of neat $CH_3NH_3PbI_3$ (4.47×10^{-9} A). Consequently, the ON/OFF ratio of $CH_3NH_3PbI_3$/rGO is 168, about 6 times higher than the $CH_3NH_3PbI_3$ photodetector (ON/OFF = 23.5). Noticeably, the responsivity[32] of the $CH_3NH_3PbI_3$/rGO photodetector reaches 73.9 mA W^{-1},

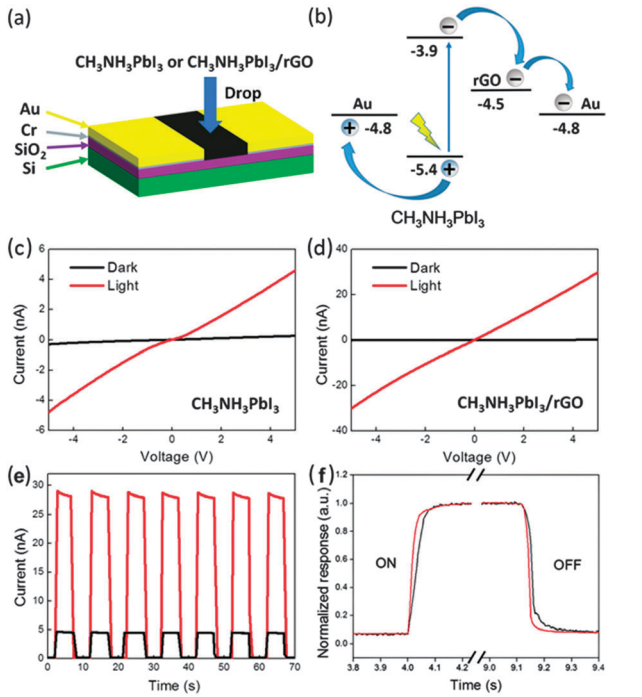

Fig. 5 Schematic diagrams of (a) the fabrication of organic–inorganic perovskite based photodetectors and (b) energy levels (eV *versus* vacuum level) in $CH_3NH_3PbI_3$/rGO hybrids for photodetector applications. *I–V* curves of (c) $CH_3NH_3PbI_3$ and (d) $CH_3NH_3PbI_3$/rGO in the dark and under light illumination at 520 nm with an intensity of 3.2 mW cm^{-2}. Time response behaviours of the $CH_3NH_3PbI_3$ (black line) and $CH_3NH_3PbI_3$/rGO (red line) photodetectors on the time scale of (e) 0–70 s and (f) 3.8–9.4 s.

representing a 6-fold improvement compared with that of $CH_3NH_3PbI_3$ (11.1 mA W^{-1}). Moreover, Fig. 5e shows seven-cycle curves of photocurrent time response under an ON/OFF interval of 5 s illumination. It is worth noting that photocurrents are all consistent and repeatable with fast responses. Noticeably, the $CH_3NH_3PbI_3$/rGO photodetector switches much faster than the $CH_3NH_3PbI_3$ photodetector from the typical ON/OFF cycle as indicated in Fig. 5f. The rise time and decay time are defined as when the photocurrent and the dark current increase or decrease by 90% compared to their stable value, respectively. Thus, the rise time (40.9 ms) and the decay time (28.8 ms) of the $CH_3NH_3PbI_3$/rGO photodetector are shorter than those of the neat $CH_3NH_3PbI_3$ photodetector (about 53.5 and 69.6 ms, respectively). The dependence of photodetector performance on the rGO amount is currently under investigation.

In conclusion, we have demonstrated a facile and versatile solution method for *in situ* synthesis of free-standing $CH_3NH_3PbI_3$/rGO hybrids, thereby forming p–n molecular junctions. Consequently, $CH_3NH_3PbI_3$/rGO particles displayed a larger size of ~1 μm than neat $CH_3NH_3PbI_3$ crystals of ~200 nm. Moreover, the maximum PL intensity of the $CH_3NH_3PbI_3$/rGO hybrids was remarkably quenched compared to that of neat $CH_3NH_3PbI_3$, indicating the efficient charge transfer between $CH_3NH_3PbI_3$ and graphene. Photodetectors based on these $CH_3NH_3PbI_3$/rGO hybrids exhibited a 6 times higher ON/OFF ratio and notably faster response speed than that based on neat $CH_3NH_3PbI_3$. Our work offers an effective and controllable strategy for *in situ* synthesis of perovskite nanocomposites.

This work was supported by National Natural Science Foundation of China (NSFC) under grant No. 51473036.

Notes and references

1 H.-S. Kim, C.-R. Lee, J.-H. Im, K.-B. Lee, T. Moehl, A. Marchioro, S.-J. Moon, R. Humphry-Baker, J.-H. Yum, J. E. Moser, M. Grätzel and N.-G. Park, *Sci. Rep.*, 2012, **2**, 591.
2 C. Wehrenfennig, G. E. Eperon, M. B. Johnston, H. J. Snaith and L. M. Herz, *Adv. Mater.*, 2014, **26**, 1584.
3 J. H. Noh, S. H. Im, J. H. Heo, T. N. Mandal and S. I. Seok, *Nano Lett.*, 2013, **13**, 1764.
4 T. Leijtens, S. D. Stranks, G. E. Eperon, R. Lindblad, E. M. J. Johansson, I. J. McPherson, H. Rensmo, J. M. Ball, M. M. Lee and H. J. Snaith, *ACS Nano*, 2014, **8**, 7147.
5 Q. Dong, Y. Fang, Y. Shao, P. Mulligan, J. Qiu, L. Cao and J. Huang, *Science*, 2015, **347**, 967.
6 L. Wang, C. McCleese, A. Kovalsky, Y. Zhao and C. Burda, *J. Am. Chem. Soc.*, 2014, **136**, 12205.
7 J.-H. Im, I.-H. Jang, N. Pellet, M. Grätzel and N.-G. Park, *Nat. Nanotechnol.*, 2014, **9**, 927.
8 X. Hu, X. Zhang, L. Liang, J. Bao, S. Li, W. Yang and Y. Xie, *Adv. Funct. Mater.*, 2014, **24**, 7373.
9 H.-R. Xia, J. Li, W.-T. Sun and L.-M. Peng, *Chem. Commun.*, 2014, **50**, 13695.
10 Y. Chen, J. Peng, D. Su, X. Chen and Z. Liang, *ACS Appl. Mater. Interfaces*, 2015, **7**, 4471.
11 L. Dou, Y. M. Yang, J. You, Z. Hong, W.-H. Chang, G. Li and Y. Yang, *Nat. Commun.*, 2014, **5**, 5404.
12 Y. Guo, C. Liu, H. Tanaka and E. Nakamura, *J. Phys. Chem. Lett.*, 2015, **6**, 535.
13 R. Dong, Y. Fang, J. Chae, J. Dai, Z. Xiao, Q. Dong, Y. Yuan, A. Centrone, X. C. Zeng and J. Huang, *Adv. Mater.*, 2015, **27**, 1912.
14 Y. Chen, Y. Zhao and Z. Liang, *Chem. Mater.*, 2015, **27**, 1448.
15 K. Yan, Z. Wei, J. Li, H. Chen, Y. Yi, X. Zheng, X. Long, Z. Wang, J. Wang, J. Xu and S. Yang, *Small*, 2015, DOI: 10.1002/smll.201403348.
16 J. Burschka, N. Pellet, S.-J. Moon, R. Humphry-Baker, P. Gao, M. K. Nazeeruddin and M. Grätzel, *Nature*, 2013, **499**, 316.
17 M. Liu, M. B. Johnston and H. J. Snaith, *Nature*, 2013, **501**, 395.
18 Q. Chen, H. Zhou, Z. Hong, S. Luo, H.-S. Duan, H.-H. Wang, Y. Liu, G. Li and Y. Yang, *J. Am. Chem. Soc.*, 2014, **136**, 622.
19 B. Li, Y. Zhao, S. Zhang, W. Gao and M. Wei, *ACS Appl. Mater. Interfaces*, 2013, **5**, 10233.
20 F. Zhang, T. Zhang, X. Yang, L. Zhang, K. Leng, Y. Huang and Y. Chen, *Energy Environ. Sci.*, 2013, **6**, 1623.
21 X. Yang, L. Zhang, F. Zhang, Y. Huang and Y. Chen, *ACS Nano*, 2014, **8**, 5208.
22 D. Chen, Y. Zhao, Y. Chen, B. Wang, H. Chen, J. Zhou and Z. Liang, *ACS Appl. Mater. Interfaces*, 2015, **7**, 3224.
23 X. F. Gao, J. Y. Li, J. Baker, Y. Hou, D. S. Guan, J. H. Chen and C. Yuan, *Chem. Commun.*, 2014, **50**, 6368.
24 B.-W. Park, S. M. Jain, X. Zhang, A. Hagfeldt, G. Boschloo and T. Edvinsson, *ACS Nano*, 2015, **9**, 2088.
25 D. Chen, G.-S. Wang, S. He, J. Liu, L. Guo and M.-S. Cao, *J. Mater. Chem. A*, 2013, **1**, 5996.
26 Z. Xiao, Q. Dong, C. Bi, Y. Shao, Y. Yuan and J. Huang, *Adv. Mater.*, 2014, **26**, 6503.
27 Y. Lee, J. Kwon, E. Hwang, C.-H. Ra, W. J. Yoo, J.-H. Ahn, J. H. Park and J. H. Cho, *Adv. Mater.*, 2015, **27**, 41.
28 Z. Zhu, J. Ma, Z. Wang, C. Mu, Z. Fan, L. Du, Y. Bai, L. Fan, H. Yan, D. L. Phillips and S. Yang, *J. Am. Chem. Soc.*, 2014, **136**, 3760.
29 J. T.-W. Wang, J. M. Ball, E. M. Barea, A. Abate, J. A. Alexander-Webber, J. Huang, M. Saliba, I. Mora-Sero, J. Bisquert, H. J. Snaith and R. J. Nicholas, *Nano Lett.*, 2014, **14**, 724.
30 R. Gottesman, E. Haltzi, L. Gouda, S. Tirosh, Y. Bouhadana and A. Zaban, *J. Phys. Chem. Lett.*, 2014, **5**, 2662.
31 A. Kumar, S. Husale, A. K. Srivastava, P. K. Duttab and A. Dhar, *Nanoscale*, 2014, **6**, 8192.
32 X. Fang, L. Hu, K. Huo, B. Gao, L. Zhao, M. Liao, P. K. Chu, Y. Bando and D. Golberg, *Adv. Funct. Mater.*, 2011, **21**, 3907.